Research Square

Preprints are preliminary reports that have not undergone peer review.
They should not be considered conclusive, used to inform clinical practice,
or referenced by the media as validated information.

A Conserved NP Mutation Quartet Drives the Avian-to-Canine Host Jump and Establishes a Molecular Foundation for Zoonotic Adaptation

Pei Zhou

zhoupei@scau.edu.cn

College of Veterinary Medicine, South China Agricultural University

Bo Chen

College of Veterinary Medicine, South China Agricultural University

Yue Zheng

College of Veterinary Medicine, South China Agricultural University

Baoqiong Xin

College of Veterinary Medicine, South China Agricultural University

Wen Liang

College of Veterinary Medicine, South China Agricultural University

Yanting Liang

Guangdong Provincial Pet Engineering Technology Research Center, College of Veterinary Medicine, South China Agricultural University, Guangzhou, Guangdong Province

Le Li

College of Veterinary Medicine, South China Agricultural University

Yu Zhou

College of Veterinary Medicine, South China Agricultural University

Xiaoyang Chen

College of Veterinary Medicine, South China Agricultural University

Shoujun Li

SCAU

Article

Keywords:

Posted Date: February 25th, 2026

DOI: https://doi.org/10.21203/rs.3.rs-8797160/v1

License: This work is licensed under a Creative Commons Attribution 4.0 International License.
Read Full License

Additional Declarations: There is **NO** Competing Interest.

Abstract

Understanding the molecular principles of influenza A virus (IAV) host-switching remains a fundamental challenge, as many landmark spillovers occurred before the era of high-resolution genomics. Here, we demonstrate that H3N2 canine influenza virus (CIV) provides a uniquely powerful evolutionary proxy to resolve the real-time molecular logic of host-switching. As a paradigm of rapid avian-to-mammalian adaptation, CIV successfully established a stable lineage and achieved global dominance while consistently lacking the classic PB2 E627K and D701N mutations, which are typically considered prerequisites for mammalian adaptation. We identify a conserved nucleoprotein (NP) mutation quartet (T373K, A428T, R452K, and N473K) as a non-canonical adaptive axis that bypasses the traditional requirement for polymerase-specific mutations. Mechanistically, these mutations optimize the viral RNP's utilization of a previously unrecognized functional interface: residue 30 within the ANP32A Leucine-Rich Repeat (LRR) domain. While this quartet was primarily selected to exploit the I30 signature —conserved across canines, felines, ferrets, and mice—it concurrently enhances compatibility with the N30 signature shared by humans, swine, equines, and guinea pigs. This dual-track compatibility underscores how adaptation within an initial mammalian reservoir provides a potent molecular foundation for broad host-range expansion. Collectively, our findings establish the NP-ANP32A interface as a critical interspecies barrier and demonstrate that NP-mediated adaptation can serve as a pre-adaptive springboard for zoonotic transmission, offering a new dimension for monitoring the pandemic potential of avian influenza viruses.

Introduction

The 21st century has been defined by recurrent, large-scale outbreaks of zoonotic viruses, ranging from SARS-CoV, highly pathogenic avian influenza viruses (HPAIVs), and the 2009 H1N1 influenza to MERS-CoV, Ebola virus, and SARS-CoV-2[1, 2, 3, 4, 5]. These events underscore the severe and persistent threat that animal-origin pathogens pose to global public health. Among these pathogens, Influenza A viruses (IAVs) warrant particular concern due to their broad host range and remarkable genetic plasticity, which drive rapid host adaptation and the recurrent emergence of mammalian-transmissible variants[6, 7, 8]. Understanding the molecular trajectories that enable avian influenza viruse (AIV) to breach species barriers remains a central challenge in viral ecology and pandemic preparedness.

Canines represent a unique clinical and ecological niche for the evolutionary consolidation of avian-origin influenza viruses. Due to the co-expression of both α-2,3- and α-2,6-linked sialic acid receptors in their respiratory tracts[9], dogs are not only highly susceptible to diverse IAV subtypes but also serve as a potent "mixing vessel" for viral reassortment[10, 11, 12, 13, 14].While both equine-origin H3N8 and avian-origin H3N2 lineages were historically established in dogs, the H3N2 canine influenza virus (CIV)—first identified in 2006—has demonstrated superior fitness[15, 16, 17, 18, 19]. It effectively outcompeted the H3N8 strain, leading to the latter's extinction in North America by 2016[20]. Intriguingly, H3N2 CIV evolved to lose infectivity in avian species while gaining the capacity to infect a broad range of mammals, including cats

and ferrets[21, 22, 23, 24]. Through sustained circulation, H3N2 CIV has acquired enhanced α-2,6-receptor binding and complete airborne transmissibility in ferrets[25]. The rapid fixation of these mammalian-adaptive traits within a single, traceable lineage characterizes H3N2 CIV as an exceptionally informative model. Consequently, this lineage provides a highly tractable and contemporary system to resolve the real-time molecular processes governing the complete avian-to-mammalian transition.

A fundamental barrier to IAV interspecies transmission is the restriction of viral polymerase activity by the host acidic nuclear phosphoprotein 32 (ANP32) family[26]. Specifically, mammalian ANP32A lacks a critical 33-amino acid insertion present in its avian ortholog, a deletion that severely impairs its ability to support avian viral polymerase complexes[27, 28]. While adaptive mutations in polymerase subunits (e.g., PB2 E627K) are well-characterized, the role of other viral components, particularly the nucleoprotein (NP), in overcoming host-specific ANP32 restriction remains poorly understood.

We identify this NP mutation quartet as a non-canonical molecular switch driving the avian-to-mammalian transition. Mechanistically, these mutations optimize the utilization of a previously unrecognized functional interface at ANP32A residue 30. Crucially, this quartet exploits the I30 signature (conserved in canines, felines, ferrets, and mice) while concurrently enhancing compatibility with the N30 signature (shared by humans, swine, equines, and guinea pigs). This dual-track compatibility defines canine adaptation as a pre-adaptive springboard for broad mammalian expansion, providing a proactive framework for monitoring zoonotic risks beyond conventional markers.

Results

H3N2 CIV gene pool is predominantly derived from Anatidae

To determine the precise avian origin and potential reassortment events of H3N2 CIV, we performed comprehensive phylogenetic analysis across all eight gene segments. The AIV dataset for this analysis incorporated sequences from all AIV subtypes for the six internal gene segments (PB2, PB1, PA, NP, M, and NS), whereas only H3 and N2 sequences were collected for the surface genes (HA and NA), respectively (see Methods).

The comprehensive phylogenetic analysis confirmed a complex reassortment origin for the H3N2 CIV. While the six internal gene segments consistently clustered with AIVs derived from various subtypes, indicating a diverse AIV gene pool contributed to the CIV genesis, all eight segments (including HA and NA) closely grouped within Eurasian lineage AIVs (Fig. 1 and Fig. S1). To pinpoint the immediate avian precursor, we utilized the earliest H3N2 CIV isolate, A/canine/Guangdong/1/2006 (CIV-GD06), for subsequent detailed analysis. The genetic evolutionary analysis, which visually distinguishes viruses recovered from Anatidae (blue branch), other avian lineages (black branches), and the H3N2 CIV lineage (red branch), clearly demonstrated the strong phylogenetic affinity: the red CIV branch primarily clustered with the blue Anatidae-origin branch. This strong clustering was further reinforced by sequence identity analysis. The sequences exhibiting the highest identity to the CIV-GD06 gene segments were

predominantly recovered from Anatidae (e.g., ducks and mallards) (Table 1 and Table S1). Specifically, both the HA and NA genes exhibited the highest identity with those of A/duck/Korea/JS53/2004 (AIV-JS53) (Table 1). Taken together, these findings strongly suggest that Anatidae served as the principal avian host and immediate genetic reservoir for the H3N2 CIV gene pool before the canine host jump.

Based on these comprehensive phylogenetic data and homology search results, we reconstructed a high-similarity avian precursor of CIV-GD06, designated AIV-N. Based on the natural isolate AIV-JS53, the putative avian precursor AIV-N was successfully rescued via multiple reverse genetics attempts. This reconstructed virus incorporates a specific combination of segments exhibiting high homology to early CIV isolates, as detailed in Fig. 2A. AIV-N exhibited a high overall nucleotide identity of 96.73% with CIV-GD06, substantially exceeding the 94.18% nucleotide identity shared with AIV-JS53. The specific amino acid differences between AIV-N and CIV-GD06 were identified and detailed in Fig. S2.

Table 1 Sequence identity analysis of HA and NA genes of CIV-GD06 with closely related AIV isolates.

Segments	GenBank Title	Accession	Identity
HA	A/duck/Korea/JS53/2004(H3N2)	JN087096.1	97.88%
	A/aquatic bird/Korea/JN-2/2006(H3N2)	EU301215.1	97.82%
	A/chicken/Korea/S6/03(H3N2)	AY862607.1	96.53%
	A/duck/Korea/JJ72/2007(H3N6)	JN087224.1	96.40%
	A/duck/Korea/KJ/2003(H3N2)	JN087020.1	96.39%
NA	A/duck/Korea/JS53/2004(H3N2)	JN087098.1	97.94%
	A/duck/Korea/S7/03(H3N2)	AY862640.1	95.96%
	A/dove/Korea/S11/03(H3N2)	AY862644.1	95.89%
	A/duck/Korea/S9/03(H3N2)	AY862642.1	95.74%
	A/duck/Hong Kong/Y439/1997(H3N2)	KF188267.1	94.82%

The table displays the five AIV strains exhibiting the highest sequence identity to the HA and NA genes of the earliest H3N2 CIV (CIV-GD06).

AIV-N retains avian-specific traits and lacks infectivity in dogs

Given that the AIV-N shares a remarkably high genomic identity (96.73%) with CIV-GD06, we sought to determine whether such a high degree of genetic similarity translates to canine infectivity. Consequently, we evaluated the host range of AIV-N, using the natural avian isolate AIV-JS53 as a positive avian control and CIV-GD06 as the benchmark for canine adaptation, through experimental infections in domestic ducks and Beagles.

In domestic ducks, AIV-N exhibited high infectivity comparable to AIV-JS53. Both viruses replicated efficiently in the respiratory and alimentary tracts (Fig. 2B), with high viral titers recovered from multiple organs at 4 days post-infection (dpi). Viral shedding was first detected in oropharyngeal and cloacal swabs at 3 dpi, and was still detectable at 7 dpi, although titers in oropharyngeal swabs were generally lower (Fig. 2C and 2D). Furthermore, histopathological analysis (HE staining) of the jejunum and rectum harvested at 4 dpi revealed cellular necrosis and sloughing caused by both AIV-JS53 and AIV-N. Abundant viral antigens were also observed in these tissues by immunohistochemistry (IHC) (Fig. 2H). In stark contrast, CIV-GD06 failed to infect the ducks, with no detectable virus presence or shedding observed in any organs or swabs throughout the experimental period. This failure was further confirmed by the absence of any notable pathological changes or viral antigen signals (IHC) in the intestinal tissues.

We next evaluated the infectivity and pathogenicity of the three viruses in dogs. The index H3N2 canine influenza virus isolate, CIV-GD06, replicated efficiently in the respiratory organs and induced clear clinical symptoms. Notably, dogs infected with CIV-GD06 exhibited a sustained febrile response; rectal temperatures rose to 39.5°C at 1 dpi and remained elevated throughout the observation period, peaking at 39.9°C by 7 dpi (Fig. S3A). In contrast, neither AIV-N nor the natural avian isolate AIV-JS53 induced fever in the infected dogs. Viral shedding patterns further reflected this difference: CIV-GD06 was detected in nasal swabs as early as 1 dpi, peaked at 5 dpi, and remained detectable at 7 dpi (Fig. 2G). Notably, neither AIV-N nor AIV-JS53 produced detectable viral titers in the respiratory organs of infected dogs. Consistent with this restricted replication, viral shedding was undetectable in nasal swabs throughout the observation period (Fig. 2E), highlighting the inability of these avian-like viruses to adapt to the canine respiratory tract. The distinct infectivity pattern was further corroborated by pathological findings. CIV-GD06 caused marked alveolar septal thickening and inflammatory cell infiltration in the lungs, along with necrosis and sloughing of tracheal mucosal epithelial cells (Fig. 2I). Abundant viral antigens were observed in these tissues by IHC. In contrast, neither AIV-N nor AIV-JS53 induced significant pathological changes or yielded detectable viral antigens in any canine respiratory tissues. Finally, the humoral immune response confirmed these results: sera collected at 14 dpi showed that CIV-GD06 infection elicited high levels of HI antibodies, whereas HI levels for AIV-JS53 and AIV-N failed to reach the threshold for seroconversion (Fig. 2F).

These data indicate that AIV-N lacks the essential molecular determinants for canine adaptation. Collectively, our findings reveal a complete host range reversal: while AIV-N is restricted in dogs, CIV-GD06 has gained robust canine infectivity while completely losing its avian infectivity. This is consistent with our previous studies showing that H3N2 CIV infects dogs but not poultry[21]. This contrast highlights the critical role of adaptive mutations in the stable establishment of H3N2 CIV in the canine population.

NP is the essential molecular determinant of H3N2 CIV adaptation

To dissect the genetic basis of H3N2 CIV adaptation, we generated eight single-gene reassortant viruses by replacing each segment of the avian precursor AIV-N with its corresponding segment from CIV-GD06.

We first evaluated these reassortants in domestic ducks to assess the impact of canine-origin genes on avian infectivity. Remarkably, the introduction of any single canine gene segment (including those encoding PB1, PA, HA, NP, NA, or M) completely abolished viral infectivity in ducks. No viral replication was detected in the trachea, lungs, or intestinal tissues (Fig. 3A), and no viral shedding was recovered from oropharyngeal or cloacal swabs throughout the 7-day observation period (Fig. 3B–C). Consistently, histopathological examination and IHC confirmed the absence of lesions and viral antigens in all avian tissues at 4 dpi (Fig. 3G).

In contrast, these reassortants exhibited varying degrees of replication in the canine respiratory tract. While segments such as PB1, PA, HA, NA, and M supported limited replication, the reassortant rN-CIV-NP fully recapitulated the high-pathogenicity phenotype of CIV-GD06. rN-CIV-NP replicated to high titers in the nasal turbinates, trachea, and lungs at 4 dpi (Fig. 3D) and exhibited sustained viral shedding in nasal swabs until 7 dpi, matching the profile of the canine parental virus (Fig. 3F). Clinically, rN-CIV-NP induced a robust and sustained febrile response (rectal temperatures >39.5°C) until 6 dpi, whereas other reassortants showed minimal or no fever (Fig. S3B). The superior infectivity of rN-CIV-NP was further evidenced by peak HI antibody titers at 14 dpi (Fig. 3E) and abundant viral antigens in canine respiratory tissues (Fig. 3H).

Collectively, these findings establish that the NP segment is the essential molecular determinant of H3N2 CIV adaptation to the canine host. While other reassortant segments permit marginal viral presence in internal respiratory tissues, they fail to reach the critical replication threshold necessary for nasal shedding. In sharp contrast, the acquisition of canine NP alone confers the high-magnitude replication and robust shedding required to bridge the species barrier. By enabling this transition from restricted tissue infection to sustained animal-to-animal transmission, NP stands out not merely as a facilitator, but as the defining driver that catalyzed the emergence and evolutionary success of the H3N2 CIV lineage.

A conserved NP mutation quartet mediate host jump from avian to canine

Building upon the finding that NP is the critical determinant of canine adaptation, we compared the NP sequences of AIV-N and CIV-GD06. This analysis, combined with a global frequency assessment of H3N2 AIV and CIV isolates, identified five candidate sites (NP 105, 373, 428, 452, and 473) where avian-like residues were nearly absent in canine strains, suggesting strong selective pressure during host adaptation (Fig. 4A). To systematically assess these sites, we rescued a library of 5 single-, 10 double-, 10 triple-, and 5 quadruple-mutant viruses on the AIV-N backbone.

Infectivity assays in both host models revealed that all single, double, and triple-mutant viruses maintained an avian-like phenotype. These viruses remained infectious in ducks but failed to establish productive infection in dogs (Fig. 4B–4M). Although marginal viral presence was detectable in some canine tissues (Fig. 4H, 4I, 4L, and 4M), these mutations were insufficient to induce sustained fever in dogs (Fig. S3C–S3E), indicating that they are inadequate for facilitating a complete host jump. Remarkably, only the quadruple-mutant virus, rN-NP-373K/428T/452K/473K (hereafter referred to as rN-

NP-4m), achieved a complete host-range shift. In ducks, this mutant totally lost infectivity, as evidenced by the absence of viral titers in organs or swabs (Fig. 4M and 4O) and a lack of lesions or viral antigens in the jejunum and rectum (Fig. 5A). In sharp contrast, rN-NP-4m exhibited robust adaptation in dogs, replicating to high titers in the respiratory tract and maintaining sustained nasal shedding comparable to CIV-GD06 (Fig. 4P and 4Q). Crucially, this infection was accompanied by sustained pyrexia (Fig. S3F), distinguishing it from the single, double, and triple mutants. Pathological analysis further confirmed severe tissue damage and abundant viral antigens in the canine trachea and lungs (Fig. 5B). Consequently, this mutant elicited the highest HI antibody titers at 14 dpi (Fig. 4R–4U), marking the functional culmination of these four key adaptive mutations.

To verify the necessity and sufficiency of these four sites, we performed two critical control experiments. First, a mutant carrying the other four differential residues (NP 105V, 109V, 260V, and 389K) failed to establish efficient canine infection, showing only minor inflammatory changes and sparse viral antigens (Fig. 4P, Q, 5B). Second, introducing the 373K/428T/452K/473K mutations into a different avian backbone, AIV-JS53, conferred effective replication and enhanced viral antigen distribution in canine respiratory tissues (Fig. 4P, Q, 5B).

Collectively, these results definitively demonstrate that the cooperative action of T373K, A428T, R452K, and N473K in the NP protein is both necessary and sufficient to mediate the avian-to-canine host jump for H3N2 influenza viruses.

Conserved NP mutation quartet is unique to H3N2 CIV and originated during canine adaptation

The acquisition of the NP mutation quartet was found to be sufficient to confer avian-to-canine host jump. To understand the evolutionary history and host specificity of these changes, we analyzed their distribution in global isolates and reconstructed ancestral sequences.

We analyzed all 34,264 available NP sequences from major influenza A virus subtypes across various hosts, including avian (AIV; H1N1, H3N2, H3N8), human (HuIV; H1N1, H3N2), swine (SIV; H1N1, H3N2), equine (EIV; H3N8), and canine (CIV; H3N2, H3N8) influenza viruses. Our analysis revealed that all four individual amino acid substitutions could be found independently and sporadically in AIV strains, likely due to random mutation. However, the simultaneous occurrence of all four NP mutations was unique to H3N2 CIV. This quadruple mutation pattern was not observed in any other analyzed influenza virus subtype or host lineage, highlighting its specificity to the canine adaptation process. Intriguingly, among the four key sites, only NP R452K demonstrated a clear avian/mammalian host demarcation (Fig. 6A-D). Avian influenza viruses universally tend to select for 452R, whereas human, swine, equine, and canine influenza viruses consistently select for NP 452K.

To determine whether these mutations were inherited or arose de novo during the host jump, we first used the Maximum Likelihood (ML) method to construct a robust phylogenetic tree for the H3N2 CIV lineage and its closely related AIV branches. This ML tree was then used to visually confirm the precise evolutionary node that represents the common ancestor between the AIV sister branches and the CIV

lineage (Fig. 6E). Subsequently, we employed the PAML software package to reconstruct the ancestral sequences at the key internal nodes. This analysis confirmed that the NP mutation quartet represents a novel adaptation event specific to the CIV lineage. Only the internal nodes and the common ancestral sequence within the CIV lineage carried the NP mutation quartet, whereas their immediate AIV sister branches did not (Fig. 6F). The posterior probabilities for these ancestral nodes all exceeded 0.95, providing strong statistical support for these findings. Notably, when these reconstructed ancestral sequences were re-integrated into the phylogenetic analysis, they correctly localized to their expected internal nodes (Fig. S4), further validating the accuracy of our evolutionary inference.

These results definitively conclude that the NP mutation quartet did not originate from a pre-adapted avian precursor, but rather emerged de novo as a conserved molecular signature that enabled H3N2 AIV to establish and persistently circulate in the canine population.

NP mutation quartet drive enhanced viral replication and cold adaptation in canine hosts

To elucidate the biological significance of the mutations identified through our in vivo canine infection experiments, we focused on the NP mutation quartet, which serves as the molecular basis for the host range shift of H3N2 AIV. We found that the emergence of the NP mutation quartet enables the parental AIV-N (originally restricted to ducks) to cross the species barrier and replicate efficiently in canine hosts. In MDCK cells (MOI = 0.5), rN-NP-4m exhibited a striking increase in replication efficiency compared to the parental AIV-N strain, reaching viral titers approximately 10-fold higher at 48 hours post-infection (hpi) and matching the growth kinetics of the canine-adapted CIV-GD06 strain (Fig. 7A).

We next dissected the functional contribution of each individual substitution using a minigenome reporter assay in HEK-293T cells (Fig. 7B). Our data revealed a clear functional dichotomy: four specific substitutions (T373K, A428T, R452K, and N473K) each significantly augmented polymerase activity, whereas the remaining four residues (I105V, I109V, A260V, and R389K) yielded negligible effects. This identifies the former four residues as the primary drivers of transcription-replication complex activity in mammalian cells.

As the transition from avian to mammalian hosts requires the virus to function at lower temperatures, we evaluated the polymerase activity of the NP mutation quartet across a temperature gradient (Fig. 7C). Compared to the parental AIV-N, the NP mutation quartet significantly bolstered polymerase activity at cooler temperatures, with a 10.01-fold enhancement observed at 35°C. To establish the physiological relevance of this improved cold adaptation, we performed in vivo thermometry of the canine nasal cavity (Fig. 7D). The internal temperature averaged 34.97°C (median 35°C), precisely aligning with the optimal temperature for the mutant's fitness gain.

In summary, these results demonstrate that the NP mutation quartet selected during canine infection specifically overcome the thermal barrier of the canine respiratory tract, facilitating the host range shift of H3N2 AIV from ducks to dogs by optimizing polymerase activity at physiological temperatures.

The NP mutation quartet mediates host adaptation by specifically utilizing canine ANP32A

To identify the host factor supporting the enhanced polymerase activity of the NP mutation quartet (373K/428T/452K/473K), we performed minigenome assays in ANP32A/B/E-triple knockout (TKO) 293T cells (Fig. 8A-C). While the NP mutation quartet did not impact duck ANP32A (DkANP32A) supported activity, it significantly bolstered activity when the avian-specific 33-amino-acid (33aa) insertion was removed (DkANP32A-△33aa), yielding a 2.91-fold increase over parental AIV-N. A consistent 2.80-fold enhancement was observed with canine ANP32A (CaANP32A), which naturally lacks the 33aa insertion (Fig. 8A). Notably, neither AIV-N nor the quadruple mutant was supported by duck or canine ANP32B or ANP32E (Fig. 8B-C). Furthermore, the NP mutation quartet consistently enhanced polymerase activity supported by ANP32A and ANP32B from humans (HuANP32A/B), swine (SwANP32A/B), and equine (EqANP32A/B), whereas the activity remained unchanged when supported by the corresponding ANP32E isoforms (Fig. 8D). Using strand-specific qPCR, we further dissected the replication cycle and confirmed that this functional potentiation was underpinned by significantly elevated levels of vRNA, cRNA, and mRNA (3.05- to 5.85-fold) (Fig. 8E). Mechanistically, Co-IP assays demonstrated that these increases were driven by a strengthened physical interaction between the mutant NP and CaANP32A (Fig. 8F). Across all assays, the quadruple mutant and the single-gene reassortant rN-CIV-NP exhibited identical phenotypic trends.

Together, these results demonstrate that the NP mutation quartet functions as a potent molecular driver that strengthens the physical interaction between NP and mammalian ANP32A. By circumventing the requirement for the avian-specific 33aa insertion, these mutations robustly enhance all stages of viral RNA synthesis across a broad range of mammalian hosts, including canines, humans, swine, and equines.

Residue 30 of the LRR Domain Governs NP–ANP32A Compatibility.

To pinpoint the specific molecular determinants within ANP32A that facilitate the enhanced activity of the NP mutation quartet, we first performed a sequence alignment between DkANP32A and CaANP32A (Fig. 9A). Domain-swapping experiments revealed that replacing the Leucine-Rich Repeat (LRR) domain of DkANP32A-△33aa with its canine counterpart (CaLRR) was sufficient to markedly increase polymerase activity, whereas the LCAR domain swap had negligible effects (Fig. 9B). Within the LRR domain, three key amino acid differences were identified: K4D, Y30I, and G104S. Notably, the Y30I substitution alone in the DkANP32A-△33aa scaffold successfully recapitulated the high-activity phenotype of the CaLRR chimera (Fig. 9C). Conversely, the reverse mutation (I30Y) in the CaANP32A LRR significantly attenuated the activity of the NP mutation quartet while leaving the parental AIV-NP unaffected, confirming the necessity of this residue for NP-mediated adaptation (Fig. 9E).

Phylogenetic analysis of ANP32A orthologs across diverse species showed that avian and mammalian sequences form distinct evolutionary clusters (Fig. 9D). While avian ANP32A (duck and chicken) possesses a conserved tyrosine (Y30), we found that mammals harbor either isoleucine (I30 in canines, felines, ferrets, and mice) or asparagine (N30 in humans, swine, horses, and guinea pigs). Functional

validation demonstrated that both Y30I and Y30N substitutions in DkANP32A-△33aa effectively supported the NP mutation quartet's activity (Fig. 9F).

These findings suggest that the emergence of H3N2 CIV in canines provided a unique evolutionary bridge; the NP mutations selected by the canine-specific I30 signature concurrently conferred broad-spectrum compatibility with the N30 signature, explaining why CIV was intrinsically capable of infecting cats, ferrets, mice, and guinea pigs upon its initial emergence.

Discussion

The Remarkable genetic plasticity of IAVs facilitates frequent host-switching events with pandemic potential[29, 30]. H3N2 CIV serves as a definitive paradigm of this process, illustrating the rapid, de novo establishment of an avian-origin virus in a novel mammalian niche. A fundamental challenge in viral evolutionary biology is that many landmark host-shifts—such as those into humans, swine, and horses—occurred before the era of high-resolution genomics, leaving their early "cold-start" trajectories largely obscured. While contemporary spillovers, such as the H5N1 outbreak in dairy cattle, are monitored via modern surveillance, they often remain experimentally constrained by the massive scale, prohibitive costs, and logistical hurdles inherent in large-animal research. In contrast, the H3N2 CIV system provides a uniquely powerful and accessible framework to resolve the real-time molecular logic of host-switching. By capturing the complete transition from a transient spillover to a stable, lineage-specific circulation, the CIV model effectively bridges the gaps inherent in other mammalian models, offering a “high-resolution window” into how viruses conquer entirely unfamiliar host environments.

Phylogenetic and experimental evidence identify Anatidae, rather than gallinaceous poultry, as the most likely source of the H3N2 CIV ancestor. Notably, AIV-JS53 is the most proximal avian relative regarding both HA and NA genes, supporting the *en bloc* acquisition of these glycoproteins[31]. Unlike the transient shedding in chickens, ducks support sustained AIV-JS53 replication[32]. Crucially, the acquisition of the NP mutation quartet enables robust replication in canines, and the H3N2 CIV genome still retains a distinctive "evolutionary imprint" of duck-like codon usage[33]. This molecular legacy suggests that ducks provided the ecological theater for the cryptic circulation and pre-adaptive diversification necessary for the virus to eventually transcend the species barrier.

Our ancestral reconstruction reveals that this conserved NP mutation quartet was fixed early in the most recent common ancestor (MRCA) of H3N2 CIV, likely during a period of cryptic circulation before the first recognized outbreaks. While R452K is observed in other mammalian IAVs, this specific quartet remains a unique signature of the H3N2 CIV lineage. The early fixation of these mutations suggests that the virus did not merely 'stumble' into canines; rather, it underwent a systematic molecular optimization. Crucially, as these mutations enhance the utilization of ANP32A across diverse mammals—including humans, swine, and horses—this early evolutionary event established a pre-adapted genetic foundation. This implies that the 'springboard' effect was encoded into the virus’s genome at the very onset of its mammalian history, providing a molecular template for rapid viral saltation.

Traditionally, studies on IAV host adaptation have prioritized HA or the polymerase complex (PB2, PB1, PA) as the primary determinants of transmission. While NP is essential for vRNP assembly[34, 35, 36, 37, 38, 39], its role as a direct driver of host-range expansion remains underappreciated. Notably, H3N2 CIV successfully established its initial lineage and global dominance while consistently lacking the classic PB2 E627K or D701N mutations, which are typically considered prerequisites for mammalian adaptation[27, 40]. Our findings identify NP as a non-canonical adaptive axis that bypasses the traditional requirement for classic polymerase mutations. Specifically, we demonstrate that a conserved NP mutation quartet provides a potent mechanism to not only overcome the host restriction mediated by the I30 signature (conserved in canines, felines, ferrets, and mice), but also concurrently enhance polymerase activity via the N30 residue (conserved in humans, swine, horses, and guinea pigs). This dual-track compatibility suggests that viral adaptation within an initial mammalian reservoir—such as the I30-bearing canine host—may function as a pre-adaptive springboard for broader host-range expansion across diverse mammalian lineages.

Collectively, our findings delineate a compelling model for the emergence of H3N2 CIV, where the acquisition of a conserved NP mutation quartet (T373K, A428T, R452K, and N473K) served as the engine for host-switching. We identify NP as a versatile molecular switch that exploits a previously unrecognized functional hotspot at ANP32A residue 30. This mechanism reveals that adaptation in canines can establish a pre-adapted genetic foundation that is functionally compatible with diverse mammalian hosts. By elucidating this dual-track adaptive pathway, our study suggests that monitoring efforts should account for such pre-adaptive signatures in the NP gene, which may enable avian-origin viruses to exploit conserved host factors even in the absence of traditional polymerase mutations. This perspective provides a complementary dimension for assessing the zoonotic risk posed by viruses circulating at the human-animal interface.

Methods

Ethics statement and biosafety

9-day-old SPF chicken embryos were obtained from Xinxing Dahuanong Poultry Egg Co., Ltd. (Yunfu, China). All animal experiments were approved by the Experimental Animal Welfare Ethics Committee of South China Agricultural University (approval number: 2023c030). Experiments involving live viruses were conducted in biosafety level 2 (BSL-2) laboratories at South China Agricultural University.

Cells

HEK-293T, TKO-293T (derived from HEK-293T cells with triple knockout of ANP32A, ANP32B, and ANP32E), and MDCK cells were maintained in Dulbecco's Modified Eagle's Medium (DMEM, Gibco) supplemented with 10% fetal bovine serum (FBS, Gibco) and 1% penicillin–streptomycin (Gibco) at 37°C in a humidified atmosphere containing 5% CO_2.

Viruses

The CIV-GD06 strain (txid707154) was originally isolated from a nasal swab of an infected dog in 2006 and is preserved at the Department of Veterinary Surgery, College of Veterinary Medicine, South China Agricultural University. AIV-JS53 (txid1041899), AIV-N (sequence information listed in Table 1), and the mutant viruses were generated by reverse genetics using the pHW2000 plasmid-based system.

Plasmids

Site-directed mutations in the viral gene segments were introduced via overlapping polymerase chain reaction (PCR). The coding sequences of CaANP32A (XM_072809376.1), CaANP32B (XM_038682241.1), and CaANP32E (XM_038423044.1); DkANP32A (XM_038184855.2), DkANP32B (XM_027472038.3), and DkANP32E (XM_027444476.3); HuANP32A (NM_006305.4), HuANP32B (NM_006401.3), and HuANP32E (NM_030920.5); SwANP32A (XM_003121759), SwANP32B (XM_021066477), and SwANP32E (XM_021089919); and EqANP32A (XM_001495810), EqANP32B (XM_023629723), and EqANP32E (XM_001917235) were cloned into the pCAGGS-Flag expression vector. Viral PB2, PB1, PA, and NP genes were also cloned into the pCAGGS vector. All plasmids and recombinant viruses were verified by Sanger sequencing to ensure the absence of unintended mutations.

Experimental Animals

To assess the host range of these H3N2 influenza viruses, three-week-old domestic ducks and ten-week-old beagle dogs were intranasally inoculated with 10^6 EID_{50} of virus. Each experimental group consisted of four animals. Oropharyngeal and cloacal (for ducks) or nasal (for dogs) swabs were collected at 1, 3, 5, and 7 dpi to monitor viral shedding. At 4 dpi, two animals from each group were euthanized for tissue collection, which was subsequently used for virus titration and histopathological examination. Viral titers in swabs and tissues were determined as EID_{50} values based on allantoic fluid collected 48 h after inoculation of embryonated chicken eggs, and the EID_{50} values were calculated using the Reed–Muench method, with a detection limit of 1.167 $\log_{10}$ EID_{50}/mL. Hemagglutination assays were performed using 1% chicken red blood cells. For dogs, body temperature were monitored daily throughout the experiment. At 14 dpi, sera were collected via venipuncture to determine seroconversion by the HI assay. All animals were confirmed to be negative for H3 subtype influenza virus antigens and antibodies prior to infection.

Phylogenetic and ancestral sequence reconstruction

All sequences, including influenza viral genomes and mammalian/avian ANP32A orthologs, were obtained from the NCBI database. Initially, sequences were aligned using MAFFT v7.520, and entries with incomplete or truncated genes were manually removed to ensure high-quality downstream analysis. Following this quality control step, the top 200 AIV sequences exhibiting the highest nucleotide identity to CIV-GD06 were identified via BLAST. To ensure broad ecological representation while minimizing computational redundancy, the remaining H3N2 AIV entries in the database were clustered at a 95% identity threshold using CD-HIT. These selected sequences and representative cluster centroids were then combined with H3N2 CIV isolates for phylogenetic reconstruction. Phylogenetic relationships were inferred using IQ-TREE (v2.3.6) under the ML framework, with the optimal substitution model

automatically determined by ModelFinder. Branch support was rigorously assessed using 1,000 replicates of both the UFBoot and the SH-aLRT. To evaluate amino acid variability within the NP gene across diverse lineages, we assembled a comprehensive global dataset comprising NP sequences from avian (H1N1, n = 493; H3N2, n = 436; H3N8, n = 1,236), human (H1N1, n = 8,827; H3N2, n = 13,689), swine (H1N1, n = 5,610; H3N2, n = 2,243), and equine (H3N8, n = 171) influenza viruses, alongside avian-origin H3N2 CIVs (n = 340) and equine-origin H3N8 CIVs (n = 70). Furthermore, the ancestral NP sequence of H3N2 CIV was reconstructed using baseml in PAML v4.10.9, specifically targeting the internal node representing the most recent common ancestor (MRCA) of the CIV clade and its avian sister clade identified in the ML tree.

Generation of recombinant viruses by reverse genetics

The gene segments of CIV-GD06 were amplified from allantoic fluid of infected embryonated chicken eggs, whereas those of AIV-N and AIV-JS53 were obtained by gene synthesis (Tsingke, China). HEK-293T and MDCK cells were seeded in 12-well plates at a 5:1 ratio. When the cells reached approximately 80% confluence, eight pHW2000 plasmids encoding each viral gene segment were cotransfected using Lipo3000 Transfection Reagent (Glpbio, USA). The cells were then incubated at 37°C in a 5% CO_2 atmosphere for 48 h. The supernatants were collected and inoculated into SPF embryonated chicken eggs. After 48 h of incubation, hemagglutination assays using 1% chicken red blood cells were performed to confirm the successful generation of recombinant viruses. Each rescued virus was verified for sequence integrity and accuracy by Sanger sequencing (Sangon, China).

Viral growth kinetics in MDCK cells

Viral titers were determined in MDCK cells by calculating the $TCID_{50}$. Serial semi-logarithmic dilutions of each virus stock were prepared, and 100 µL of each dilution was inoculated into MDCK monolayers in 96-well plates, with five replicate wells per dilution. Plates were incubated at 37°C in a 5% CO_2 atmosphere for 1 h, with gentle shaking every 30 min. After incubation, the inoculum was removed, and 100 µL of virus growth medium containing 0.5 g/mL tosylsulfonyl phenylalanyl chloromethyl ketone (TPCK)–trypsin was added to each well. Following 48 h of incubation, $TCID_{50}$ values were calculated using the Reed–Muench method. For viral replication kinetics, MDCK cells were infected at a MOI of 0.05 and incubated in virus growth medium supplemented with 0.5 µg/mL TPCK–trypsin for 8, 12, 24, and 48 h. Supernatants collected at each time point were titrated in embryonated chicken eggs to determine the EID50 values.

Polymerase activity assays

To assess the effects of NP point mutations on viral polymerase activity in mammalian host cells, a dual-luciferase reporter assay was employed to compare the polymerase activities of vRNP complexes carrying different NP mutations. HEK-293T cells were cotransfected with PB2 (100 ng), PB1 (100 ng), PA (100 ng), NP (100 ng), 5 ng of the Renilla luciferase expression plasmid (pRL-TK), and 100 ng of the minigenome reporter plasmid (pHH21-huPolI-vLuc), in which the Firefly luciferase gene is flanked by the noncoding regions of the H3N2 CIV NP gene. Transfection was performed using Lipo3000 Transfection

Reagent (Glpbio, USA). At 24 h posttransfection, luciferase activities were measured using a Dual-Luciferase Reporter Assay System (Yeasen, China) and a GloMax luminometer (Promega, USA).

To elucidate the relationship between the NP mutation quartet and host ANP32 proteins, expression plasmids encoding canine or duck ANP32 proteins (10 ng) were cotransfected into TKO-293T cells along with the vRNP complexs, pRL-TK, and pHH21-huPolI-vLuc. Firefly and Renilla luciferase activities were then measured to assess how the NP mutation quartet influenced polymerase activity supported by different host ANP32 proteins.

Quantification of viral RNAs by real time PCR

This experiment was conducted under the same transfection conditions as the polymerase activity assay described above. In TKO-293T cells, CaANP32A plasmid was cotransfected with the vRNP complex and pHH21-huPolI-vLuc. At 24 h post-transfection, total RNA was extracted using the Total RNA Extraction Kit (Fastagen, China). First-strand cDNA was synthesized from the extracted RNA with the HiScript II 1st Strand cDNA Synthesis Kit (Vazyme, China). The uni12 primer (5'-AGCAAAAGCAGG-3') was used to reverse transcribe Firefly luciferase vRNA, the primer 5'-AGTAGAAACAAGG-3' for Firefly luciferase cRNA, and oligo(dT) for Firefly luciferase mRNA. Quantitative real-time PCR was then performed using ChamQ Blue Universal SYBR qPCR Master Mix (Vazyme, China) with specific primers F (5'-ACTGGGACGAAGACGAACAC-3') and R (5'-GGCGACGTAATCCACGATCT-3').

Immunoprecipitation assay

pCAGGS-Flag-CaANP32A plasmids were cotransfected with pCAGGS-NP or pCAGGS empty vector into TKO-293T cells. Twenty-four hours post-transfection, cells were lysed on ice using Western and IP cell lysis buffer (NCM, China) containing protease and phosphatase inhibitors (NCM, China) and centrifuged at 13,000 × g for 10 min at 4°C. The supernatants were precleared for 12 h at 4°C using magnetic beads (MCE, USA) conjugated with mouse IgG antibody (Beyotime, China). After magnetic separation, the cleared lysates were incubated with magnetic beads prebound to mouse Flag antibody (Proteintech, China) at 4°C for 4 h. All beads were collected, and after discarding the supernatant, SDS-PAGE loading buffer was added and samples were boiled for 5 min before SDS-PAGE and Western blot analysis. Signals were detected using the Odyssey Imaging System (LI-COR, USA). The NP antibody used in this study was GTX125989 (Genetex, USA).

Statistics

Data analysis was performed using GraphPad Prism version 8 (GraphPad Software, USA). Statistical significance was assessed by ANOVA. Error bars represent either the SD or the SEM, as indicated in the Fig.ure legends. *$p < 0.05$; **$p < 0.01$; ***$p < 0.001$; ns, $p > 0.05$. All experiments were independently conducted in triplicate.

Declarations

Data availability

All data generated in this study are provided within the Article and its Supplementary Information files. The viral sequence data analyzed in this study were obtained from the NCBI database.

Competing interests

The authors declare no competing interests.

Author contributions

Conceptualization, Pei Zhou; Methodology, Bo Chen; Investigation, Bo Chen, Yue Zheng, Baoqiong Xin, Wen Liang, Yanting Liang, Le Li, Yu Zhou, and Xiaoyang Chen; Formal Analysis, Bo Chen; Data Curation, Bo Chen; Writing – Original Draft, Bo Chen; Writing – Review & Editing, Pei Zhou; Resources, Shoujun Li; Supervision, Pei Zhou and Shoujun Li; Funding Acquisition, Pei Zhou.

Acknowledgments

This work was supported by the Natural Science Foundation of Guangdong Province, China (2025A1515010900).

References

1. Ge XY et al (2013) Isolation and characterization of a bat SARS-like coronavirus that uses the ACE2 receptor. Nature 503:535–538
2. Garten RJ et al (2009) Antigenic and genetic characteristics of swine-origin 2009 A(H1N1) influenza viruses circulating in humans. Sci (New York NY) 325:197–201
3. Zaki AM, Boheemen Sv, Bestebroer TM, Osterhaus ADME, Fouchier RAM (2012) Isolation of a Novel Coronavirus from a Man with Pneumonia in Saudi Arabia. 367:1814–1820
4. Holmes EC et al (2021) The origins of SARS-CoV-2: A critical review. Cell 184:4848–4856
5. Gao R et al (2013) Human infection with a novel avian-origin influenza A (H7N9) virus. N Engl J Med 368:1888–1897
6. Chou YY, Vafabakhsh R, Doğanay S, Gao Q, Ha T, Palese P (2012) One influenza virus particle packages eight unique viral RNAs as shown by FISH analysis. Proc Natl Acad Sci USA 109:9101–9106
7. Trovão NS, Khan SM, Lemey P, Nelson MI, Cherry JL (2024) Comparative evolution of influenza A virus H1 and H3 head and stalk domains across host species. mBio 15:e0264923

8. Long JS, Mistry B, Haslam SM, Barclay WS (2019) Host and viral determinants of influenza A virus species specificity. Nat Rev Microbiol 17:67–81
9. Ning ZY et al (2012) Tissue distribution of sialic acid-linked influenza virus receptors in beagle dogs. J Vet Sci 13:219–222
10. Songserm T et al (2006) Fatal avian influenza A H5N1 in a dog. Emerg Infect Dis 12:1744–1747
11. Lin HT, Wang CH, Chueh LL, Su BL, Wang LC, Influenza (2015) A(H6N1) Virus in Dogs, Taiwan. Emerg Infect Dis 21:2154–2157
12. Sun X et al (2013) Evidence of avian-like H9N2 influenza A virus among dogs in Guangxi, China. Infect Genet evolution: J Mol Epidemiol evolutionary Genet Infect Dis 20:471–475
13. Lin D et al (2012) Natural and experimental infection of dogs with pandemic H1N1/2009 influenza virus. J Gen Virol 93:119–123
14. Chen Y et al (2015) Emergence of human-like H3N2 influenza viruses in pet dogs in Guangxi, China. Virol J 12:10
15. Li S et al (2010) Avian-origin H3N2 canine influenza A viruses in Southern China. Infect Genet evolution: J Mol Epidemiol evolutionary Genet Infect Dis 10:1286–1288
16. Song D et al (2008) Transmission of avian influenza virus (H3N2) to dogs. Emerg Infect Dis 14:741–746
17. Bunpapong N et al (2014) Genetic characterization of canine influenza A virus (H3N2) in Thailand. Virus Genes 48:56–63
18. Voorhees IEH et al (2017) Spread of Canine Influenza A(H3N2) Virus, United States. Emerg Infect Dis 23:1950–1957
19. Xu W, Weese JS, Ojkic D, Lung O, Handel K, Berhane Y (2020) Phylogenetic Inference of H3N2 Canine Influenza A Outbreak in Ontario, Canada in 2018. Sci Rep 10:6309
20. Wasik BR et al (2023) Understanding the divergent evolution and epidemiology of H3N8 influenza viruses in dogs and horses. Virus Evol 9
21. Zhou P, Chen B, Hu X, Xiao X, Liu R, Li S (2022) Domestic poultry are not susceptible to avian-origin H3N2 subtype canine influenza A virus. Vet Microbiol 272:109501
22. Lyoo KS et al (2015) Comparative analysis of virulence of a novel, avian-origin H3N2 canine influenza virus in various host species. Virus Res 195:135–140
23. Lee YN et al (2013) Experimental infection and natural contact exposure of ferrets with canine influenza virus (H3N2). J Gen Virol 94:293–297
24. Kim H et al (2013) Inter- and intraspecies transmission of canine influenza virus (H3N2) in dogs, cats, and ferrets. Influenza Other Respir Viruses 7:265–270
25. Chen M et al (2023) Increased public health threat of avian-origin H3N2 influenza virus caused by its evolution in dogs. *eLife* 12
26. Sun L et al (2023) The SUMO-interacting motif in NS2 promotes adaptation of avian influenza virus to mammals. Sci Adv 9:eadg5175

27. Zhang H et al (2019) Fundamental Contribution and Host Range Determination of ANP32A and ANP32B in Influenza A Virus Polymerase Activity. J Virol 93
28. Long JS et al (2016) Species difference in ANP32A underlies influenza A virus polymerase host restriction. Nature 529:101–104
29. Ding X, Liu J, Jiang T, Wu A (2024) Transmission restriction and genomic evolution co-shape the genetic diversity patterns of influenza A virus. Virol Sin 39:525–536
30. Short KR et al (2015) One health, multiple challenges: The inter-species transmission of influenza A virus. One health (Amsterdam Netherlands) 1:1–13
31. Zhu H, Hughes J, Murcia PR (2015) Origins and Evolutionary Dynamics of H3N2 Canine Influenza Virus. J Virol 89:5406–5418
32. Choi JG et al (2012) Genetic relationship of H3 subtype avian influenza viruses isolated from domestic ducks and wild birds in Korea and their pathogenic potential in chickens and ducks. Vet Microbiol 155:147–157
33. Guo F et al (2021) Host Adaptive Evolution of Avian-Origin H3N2 Canine Influenza Virus. Front Microbiol 12:655228
34. Kukol A, Hughes DJ (2014) Large-scale analysis of influenza A virus nucleoprotein sequence conservation reveals potential drug-target sites. Virology 454–455:40–47
35. Coloma R et al (2020) Structural insights into influenza A virus ribonucleoproteins reveal a processive helical track as transcription mechanism. Nat Microbiol 5:727–734
36. Compans RW, Content J, Duesberg PH (1972) Structure of the ribonucleoprotein of influenza virus. J Virol 10:795–800
37. Zhu Z, Fodor E, Keown JR (2023) A structural understanding of influenza virus genome replication. Trends Microbiol 31:308–319
38. Boulo S, Akarsu H, Ruigrok RW, Baudin F (2007) Nuclear traffic of influenza virus proteins and ribonucleoprotein complexes. Virus Res 124:12–21
39. Yu M et al (2012) Identification and characterization of three novel nuclear export signals in the influenza A virus nucleoprotein. J Virol 86:4970–4980
40. Mistry B, Long JS, Schreyer J, Staller E, Sanchez-David RY, Barclay WS (2020) Elucidating the Interactions between Influenza Virus Polymerase and Host Factor ANP32A. J Virol 94
41. Sun L, Guo X, Yu M, Wang XF, Ren H, Wang X (2024) Human ANP32A/B are SUMOylated and utilized by avian influenza virus NS2 protein to overcome species-specific restriction. Nat Commun 15:10805
42. Katoh K, Standley DM (2013) MAFFT multiple sequence alignment software version 7: improvements in performance and usability. Mol Biol Evol 30:772–780
43. Nguyen LT, Schmidt HA, von Haeseler A, Minh BQ (2015) IQ-TREE: a fast and effective stochastic algorithm for estimating maximum-likelihood phylogenies. Mol Biol Evol 32:268–274
44. Yang Z (2007) PAML 4: phylogenetic analysis by maximum likelihood. Mol Biol Evol 24:1586–1591

Figures

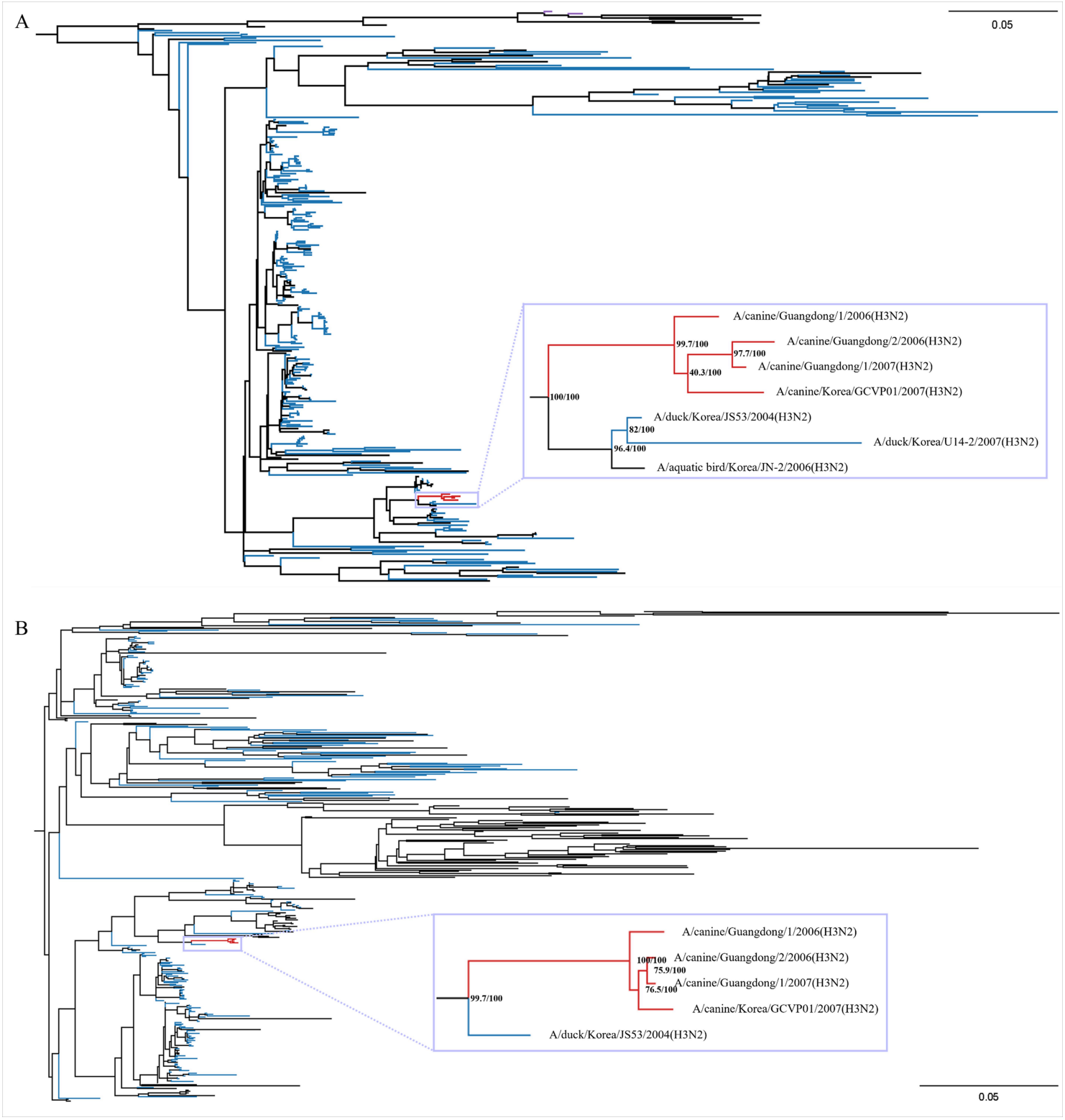


Figure 1

Phylogenetic analysis of the HA and NA genes of H3N2 CIV.

A Phylogenetic tree of the HA gene segment. **B** Phylogenetic tree of the NA gene segment. The trees illustrate the evolutionary relationships between H3N2 CIV and related AIV lineages. Branch colors represent different lineages: red, H3N2 CIV; deep purple, human H3N2 influenza viruses; blue, AIV strains from Anatidae; and black, AIV strains from other avian species. Numerical values at key nodes indicate ultrafast bootstrap (UFBoot) support and Shimodaira-Hasegawa-like approximate likelihood ratio test (SH-aLRT) percentages, respectively.

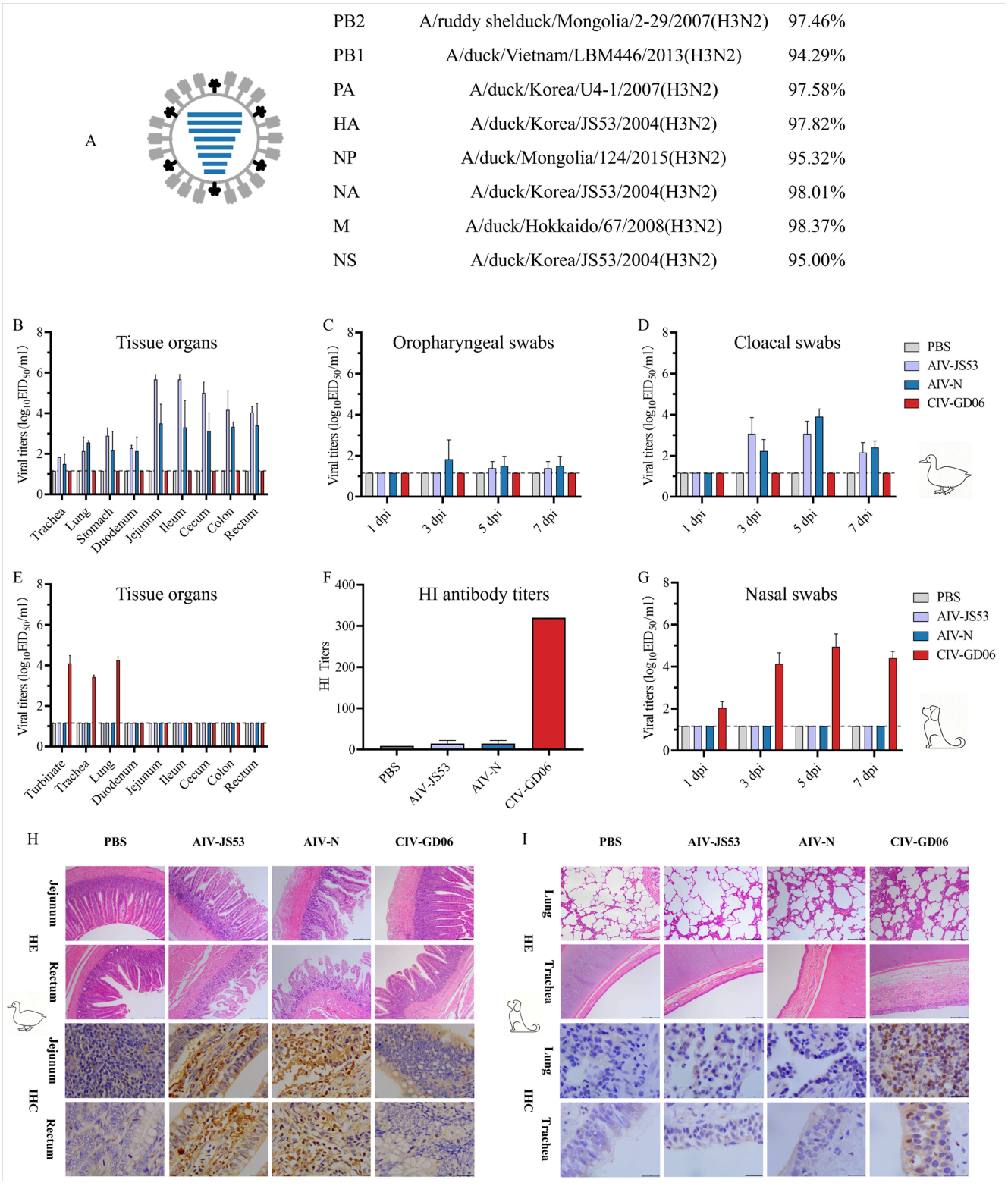


Figure 2

Host range and pathogenicity of the reconstructed AIV-N in ducks and dogs.

A Genomic composition and sequence identity of the reconstructed AIV-N. **B** Viral titers in various organs of domestic ducks collected at 4 dpi. **C** Viral shedding titers in oropharyngeal swabs of domestic ducks collected at 1, 3, 5, and 7 dpi. **D**Viral shedding titers in cloacal swabs of domestic ducks collected at 1, 3, 5, and 7 dpi. **E** Viral titers in respiratory organs of dogs collected at 4 dpi. **F** HI antibody titers in canine sera collected at 14 dpi. **G**Viral shedding titers in nasal swabs of dogs collected at 1, 3, 5, and 7 dpi. **H**Histopathological (HE) and IHC analysis of duck intestinal tissues. **I** HE and IHC analysis of canine respiratory tissues.

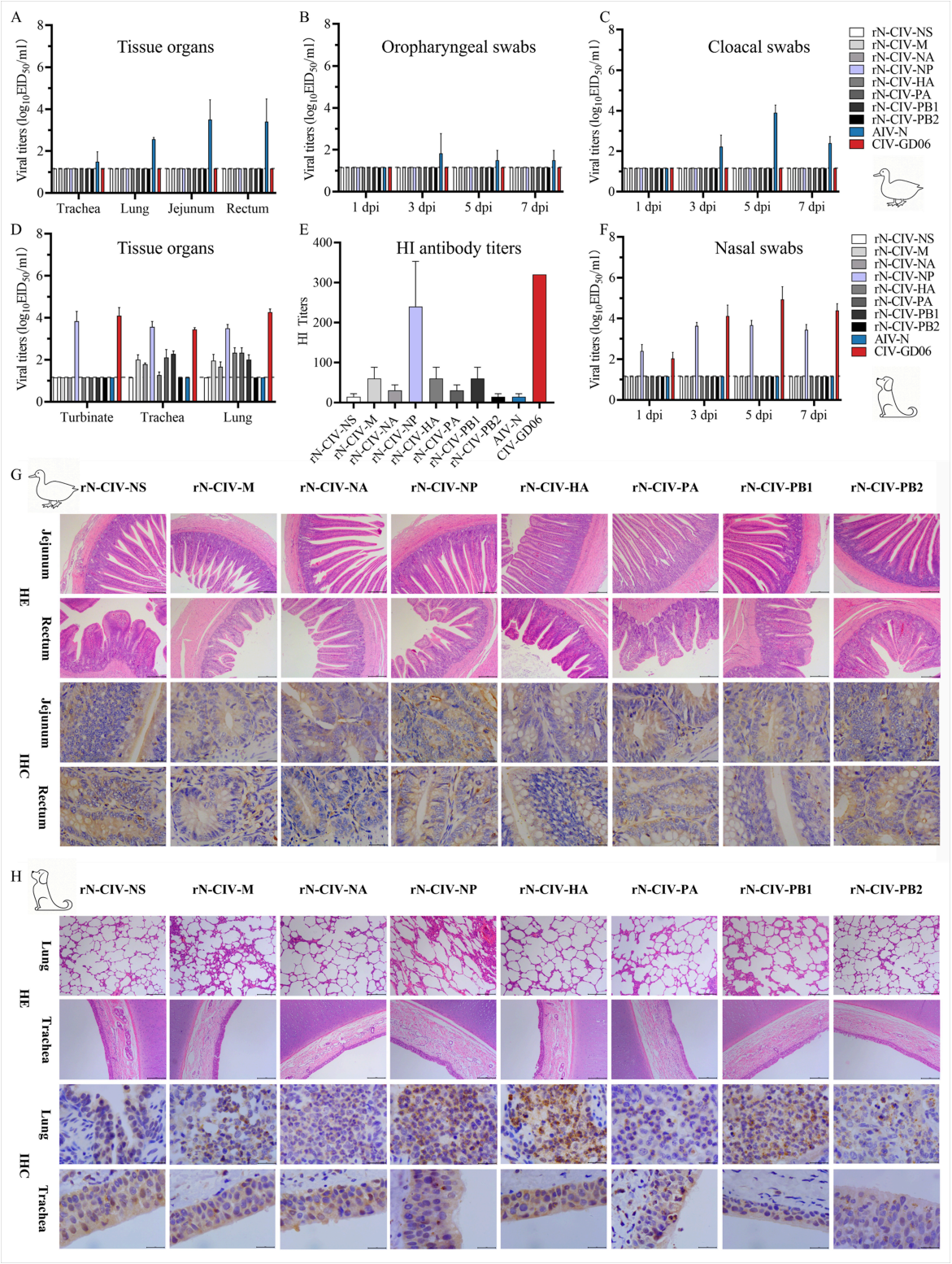


Figure 3

Identification of the NP segment as the primary determinant for the host range shift of H3N2 CIV.

A Viral titers in the trachea, lungs, jejunum, and rectum of domestic ducks collected at 4 dpi. **B** Viral shedding titers in oropharyngeal swabs of domestic ducks collected at 1, 3, 5, and 7 dpi. **C** Viral shedding titers in cloacal swabs of domestic ducks collected at 1, 3, 5, and 7 dpi. **D** Viral titers in the nasal turbinates, trachea, and lungs of dogs harvested at 4 dpi. **E** HI antibody titers in canine sera collected at 14 dpi. **F** Viral shedding titers in nasal swabs of dogs collected at 1, 3, 5, and 7 dpi. **G** Representative HE-stained and IHC-stained images of duck jejunum and rectum tissues at 4 dpi. **H**Representative HE-stained and IHC-stained images of canine trachea and lung tissues at 4 dpi.

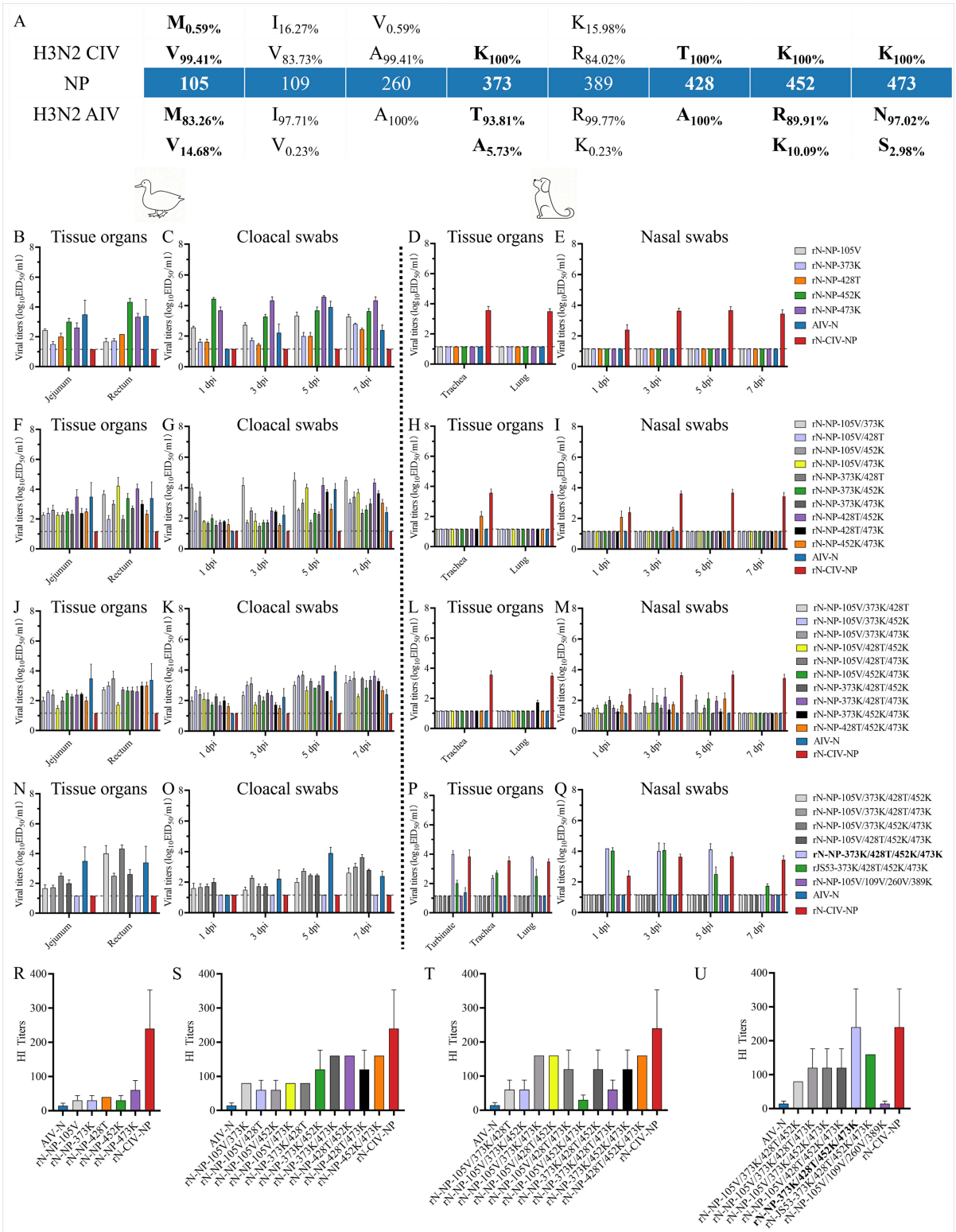


Figure 4

Identification of the key amino acid substitutions in NP that drive the host range shift of H3N2 CIV.

A Residue frequency analysis of the identified NP mutations across avian and canine influenza virus lineages. **B**Viral titers in the jejunum and rectum of domestic ducks inoculated with NP single-mutant viruses at 4 dpi. **C** Viral shedding titers in cloacal swabs of domestic ducks inoculated with NP single-mutant viruses from 1 to 7 dpi. **D**Viral titers in the trachea and lungs of dogs inoculated with NP single-mutant viruses at 4 dpi. **E** Viral shedding titers in nasal swabs of dogs inoculated with NP single-mutant viruses from 1 to 7 dpi. **F** Viral titers in the jejunum and rectum of domestic ducks inoculated with NP double-mutant viruses at 4 dpi. **G** Viral shedding titers in cloacal swabs of domestic ducks inoculated with NP double-mutant viruses from 1 to 7 dpi. **H** Viral titers in the trachea and lungs of dogs inoculated with NP double-mutant viruses at 4 dpi. **I** Viral shedding titers in nasal swabs of dogs inoculated with NP double-mutant viruses from 1 to 7 dpi. **J** Viral titers in the jejunum and rectum of domestic ducks inoculated with NP triple-mutant viruses at 4 dpi. **K** Viral shedding titers in cloacal swabs of domestic ducks inoculated with NP triple-mutant viruses from 1 to 7 dpi. **L** Viral titers in the trachea and lungs of dogs inoculated with NP triple-mutant viruses at 4 dpi. **M** Viral shedding titers in nasal swabs of dogs inoculated with NP triple-mutant viruses from 1 to 7 dpi. **N** Viral titers in the jejunum and rectum of domestic ducks inoculated with the NP quadruple-mutant virus at 4 dpi. **O** Viral shedding titers in cloacal swabs of domestic ducks inoculated with the NP quadruple-mutant virus from 1 to 7 dpi. **P** Viral titers in the trachea and lungs of dogs inoculated with the NP quadruple-mutant virus at 4 dpi. **Q** Viral shedding titers in nasal swabs of dogs inoculated with the NP quadruple-mutant virus from 1 to 7 dpi. **R**HI antibody titers in canine sera collected at 14 dpi following infection with NP single-mutant viruses. **S** HI antibody titers in canine sera collected at 14 dpi following infection with NP double-mutant viruses. **T** HI antibody titers in canine sera collected at 14 dpi following infection with NP triple-mutant viruses. **U** HI antibody titers in canine sera collected at 14 dpi following infection with the NP quadruple-mutant virus.

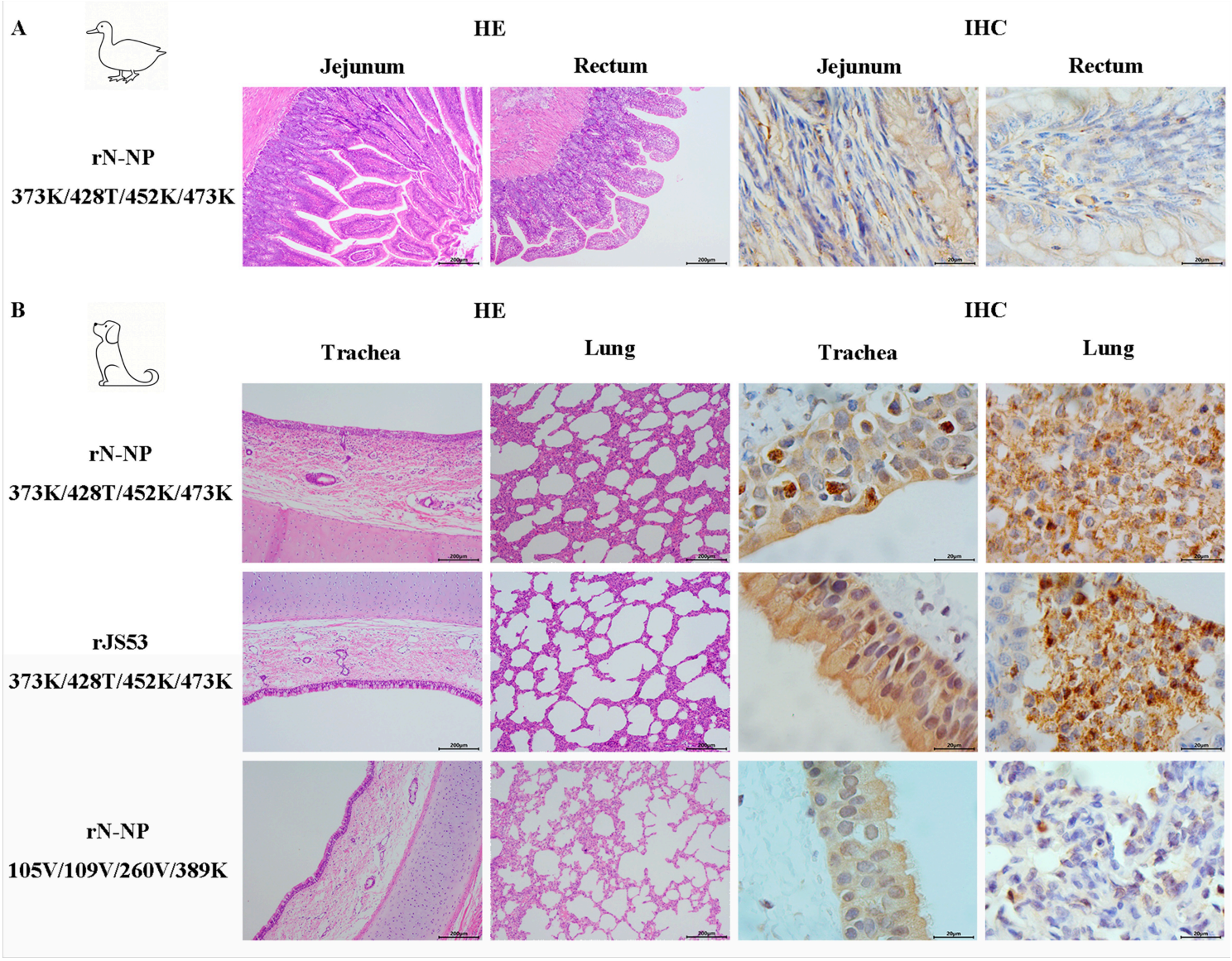
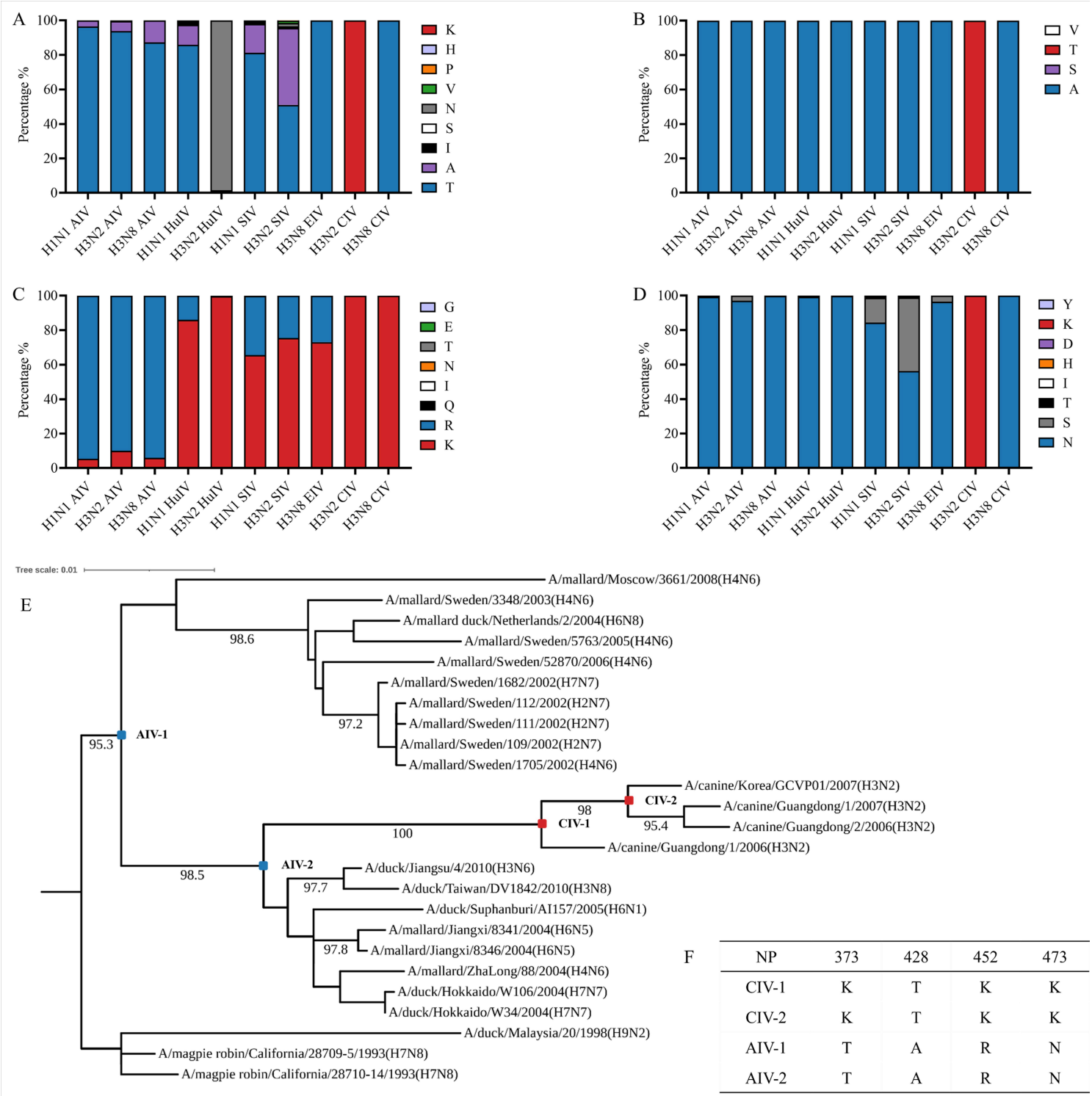


Figure 5

Histopathological and immunohistochemical analysis of key NP mutant viruses in avian and canine hosts.

A Pathological evaluation in ducks. **B** Pathological evaluation in dogs.



NP	373	428	452	473
CIV-1	K	T	K	K
CIV-2	K	T	K	K
AIV-1	T	A	R	N
AIV-2	T	A	R	N

Figure 6

Evolutionary analysis and ancestral state reconstruction of key adaptive mutations in NP.

A Residue frequency distribution at position 373 across influenza viruses isolated from human, swine, equine, canine, and avian hosts. **B** Residue frequency distribution at position 428 across influenza viruses isolated from human, swine, equine, canine, and avian hosts. **C** Residue frequency distribution at

position 452 across influenza viruses isolated from human, swine, equine, canine, and avian hosts. **D**Residue frequency distribution at position 473 across influenza viruses isolated from human, swine, equine, canine, and avian hosts. **E** Ancestral sequence reconstruction and phylogenetic analysis of the NP gene. Nodes representing key ancestral sequences are indicated, with branch support values expressed as UFBoot percentages. **F** Amino acid profiles of the reconstructed ancestral nodes at the identified adaptive positions.

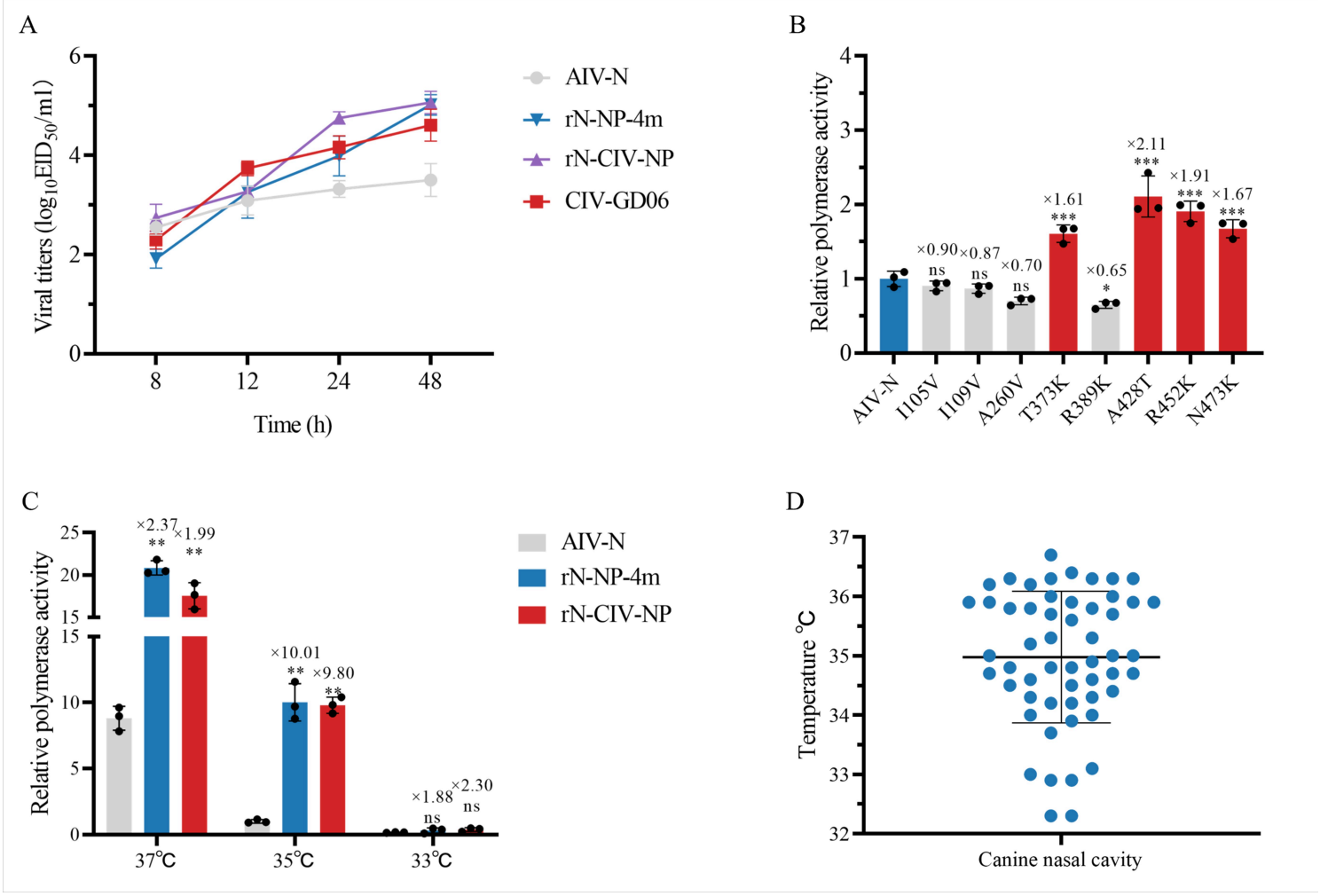


Figure 7

Functional characterization of the NP mutation quartet in viral fitness and cold adaptation.

A Viral replication kinetics in MDCK cells. **B** Polymerase activity measured by minigenome assays. **C**Temperature-dependent polymerase activity (cold adaptation). **D** Physiological temperature of the canine nasal cavity. Statistical significance was assessed by one-way analysis of variance (ANOVA). Error bars represent either the standard deviation (SD) or the standard error of the mean (SEM). *p < 0.05; **p < 0.01; ***p < 0.001; ns, p > 0.05.

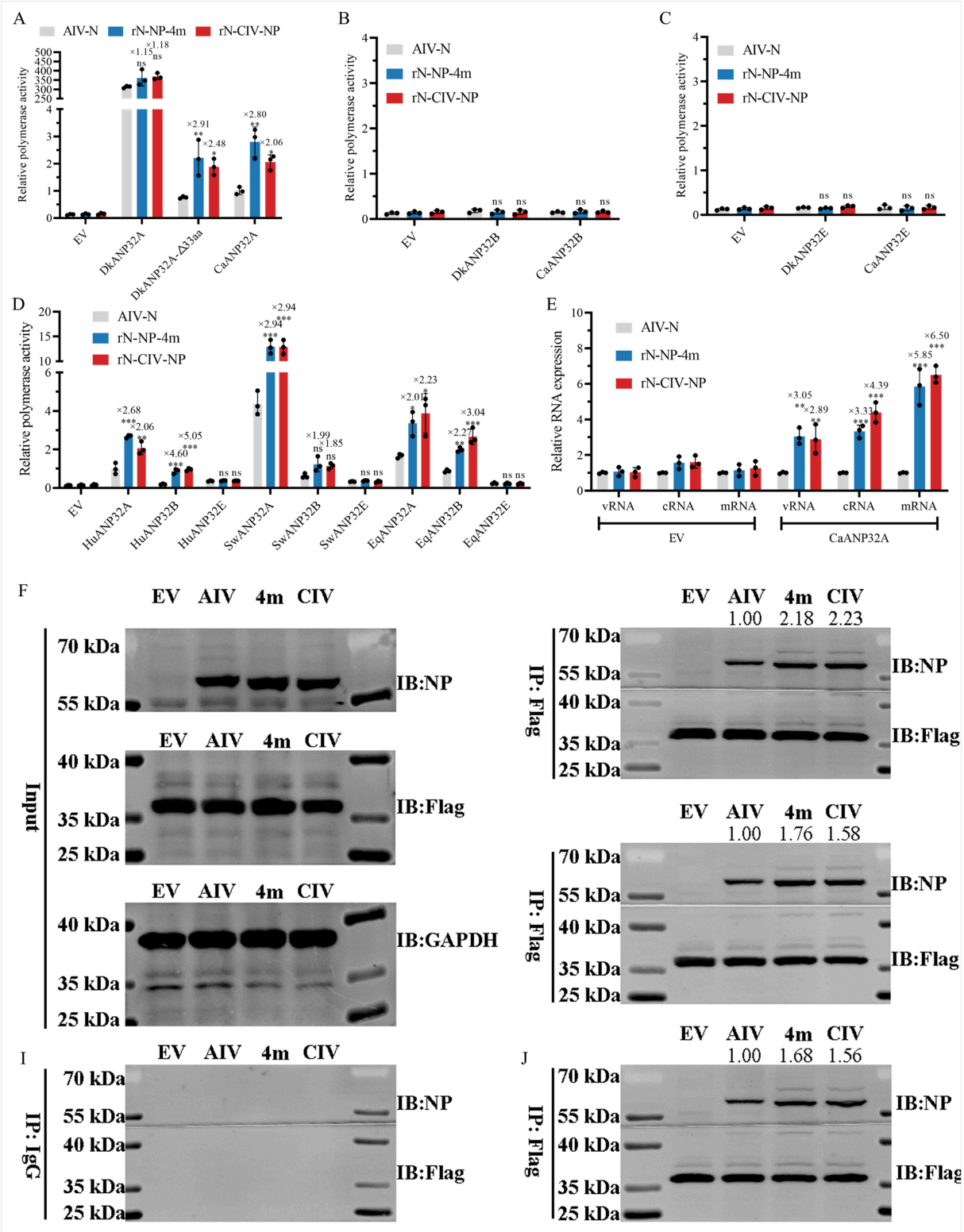


Figure 8

The NP mutation quartet overcomes host restriction by enhancing interaction with CaANP32A.

A-C Differential support of viral polymerase activity by various ANP32 isoforms. **D** Universal functional support of viral replication by diverse mammalian ANP32 orthologs. **E** Quantitative analysis of vRNA, cRNA, and mRNA levels. **F** Physical interaction between NP and CaANP32A. Statistical significance was assessed by ANOVA. Error bars represent either the SD or the SEM. *p < 0.05; **p < 0.01; ***p < 0.001; ns, p > 0.05.

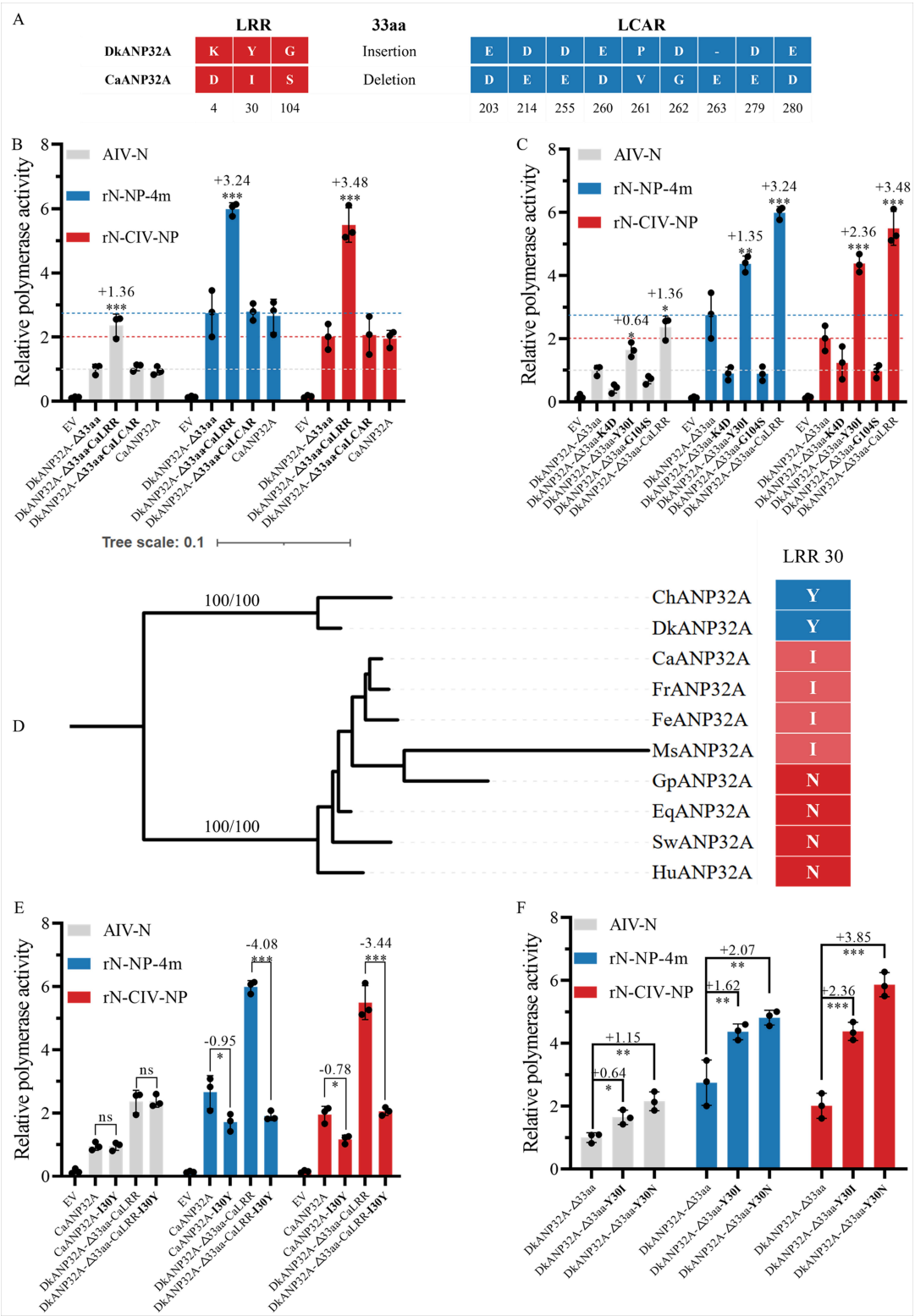


Figure 9

Residue 30 of the ANP32A LRR domain governs the host-factor dependency of the NP mutation quartet.

A Sequence alignment of ANP32A LRR and LCAR domains from duck and canine. **B** Polymerase activity of AIV-N and the NP mutation quartet supported by Dk/Ca-ANP32A chimeras. DkANP32A-△33aa served as the backbone, with LRR or LCAR domains replaced by canine counterparts. **C**Identification of the key adaptive residue within the LRR domain. Minigenome assays were performed using DkANP32A-△33aa carrying single point mutations (K4D, Y30I, or G104S). **D** Evolutionary landscape of ANP32A residue 30 across avian and mammalian species. The phylogenetic tree (left) and sequence logo (right) illustrate the divergence between the Y30 signature (found in duck and chicken), the I30 signature (found in canine, feline, ferret, and mouse), and the N30 signature (found in human, swine, horse, and guinea pig). Abbreviations: Ck, chicken (Gallus gallus); Fe, feline (Felis catus); Fr, ferret (Mustela putorius furo); Ms, mouse (Mus musculus); Gp, guinea pig (Cavia porcellus). **E** Functional necessity of residue 30. The reverse mutation I30Y was introduced into CaANP32A to assess its impact on the activity of the NP mutation quartet relative to parental AIV-NP. **F** Convergence of Y30I and Y30N signatures in supporting NP-mediated adaptation. Minigenome activity was measured using DkANP32A-△33aa variants (Y30I or Y30N) to validate the "evolutionary bridge" effect. Statistical significance was assessed by ANOVA. Error bars represent either the SD or the SEM. *$p < 0.05$; **$p < 0.01$; ***$p < 0.001$; ns, $p > 0.05$.

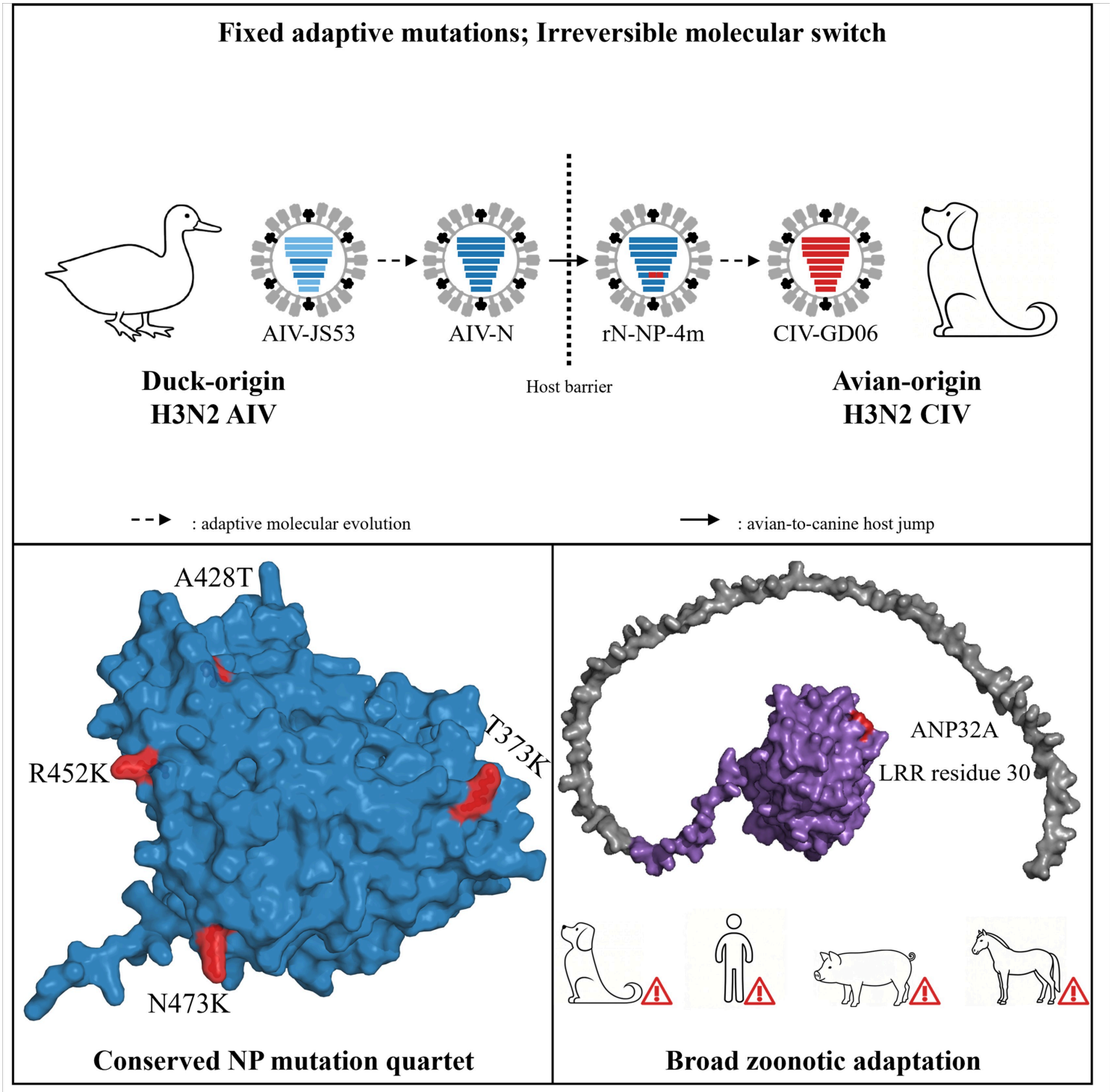


Figure 10

Evolutionary trajectory and molecular mechanism of the NP-mediated avian-to-canine host jump.

Supplementary Files

This is a list of supplementary files associated with this preprint. Click to download.

- TableS1.docx

- FigureS2.docx
- FigureS3.docx
- FigureS4.docx
- FigureS1.docx
- rs.pdf